Journal of Engineering Sciences, Assiut University, Vol. 36, No. 4, pp.841 -862 , July 2008

COOLING CHARACTERISTICS OF PARTIALLY HOLLOW FINNED PLATE EXPOSED TO JET IMPINGEMENT

***Mohamed El-sayed Gomaa*,**
Specialized Studies Academy, Workers University, Technology Dept., Ismailia, EGYPT. Email: msgomaas@hotmail.com

Abd Alla Galal Gomaa
Refr. and A/C Dept., The Faculty of Industrial Education, Helwan University, Cairo, EGYPT. Email: abdallagomaa@hotmail.com

El-Desuki Ibrahim Eid
Mech. Dept., the Faculty of Industrial Education, Suez Canal University, Suez, EGYPT. Email: eldesukieid@yahoo.com

(Received May 12, 2008 Accepted July 2, 2008)

In the present work, experimental and numerical investigations have been performed to determine the enhancement of cooling characteristics of partially hollow finned plate due to its exposure to a jet impingement. Six test specimens were designed and manufactured with a particular reference of the heat sink of a PC processor as a test specimen. The hollow shapes were cut in the central zone of the specimens by an adequate cut to form a cylindrical hole or frustum-conical holes of different vertex angles. The effects of Reynolds number, angle of attack and nozzle-to-surface distance on the enhancement of cooling characteristics have been highlighted. Empirical correlations for Nusselt number at the stagnation zone of each hollow shape were exhibited. A three-dimensional numerical simulation using the CFD FLUENT-6.2-code was applied to the case study. The validated CFD model highlights the flow characteristics through the specimens. The results show that the partially hollow finned plate has the potential to deliver a remarkably higher enhancement in the thermal performance if it is compared with those traditional ones.

KEYWORDS: *Jet impingement, Heat sink, Hollow shapes, Thermal cooling, Enhancement*

NOMENCLATURE

Symbol	***Description***	***Unit***
A	Area	m^2
a	Cross-section area of a fin	m^2
d	Diameter	*m*
grad	gradient of scalar (*grad u* = ∂u/∂x + ∂u/∂y + ∂u/∂z)	*1/s*
E	Energy	*J*
F	Shape factor	

H	Fin height	m
h	Convective heat transfer coefficient	W/m^2K
I	Electric current	*ampere*
k	Thermal conductivity	$W/m\,K$
L	Length	m
Nu	Nusselt number	
P	Perimeter of the fin cross-section	m
p	Pressure	*Pa.*
Pr	Prandtl number	
$\dot{Q}$	Heat transfer rate	W
Re	Reynolds number	
s	Pitch	m
T	Temperature	K
t	Time	s
$\mathbf{u}$	Velocity vector, $(u\vec{i}+v\vec{j}+w\vec{k})$	m/s
V	Voltage	*volt*
u, v, w	Velocity components in directions of Cartesian coordinates	m/s
W	Specimen width	m
x, y, z	Cartesian coordinates	m
α	Thermal diffusivity	m^2/s
β	Vertex angle	*Degree*
δ	Fin thickness	m
ε	Emissivity	
ϕ	Hollow shape diameter	
μ	Viscosity	*Pa.s*
θ	Angle of attack	*Degree*
ρ	Density	kg/m^3
σ	Stefan-Boltzmann constant	$W/m^2.K^4$
ξ	Enhancement ratio	

Subscripts

a	Air	f	Fin	r	Fin root
b	Bottom side of the base	f,o	Opposite fin	rad	Radiation
b,c	Base area of the cavity	g	Geometry	s	Solid (Aluminum)
c	Cavity	ins	Asbestos layer	T	Total
cond	Conduction	m	Fin mid-plane	t	Fin tip
conv	Convection	n	Nozzle exit	y	Nozzle-to-surface distance

INTRODUCTION

Cooling of heat sinks at high heat fluxes is currently a barrier to develop new techniques to overcome the heat fluxes from electronic systems such as those used in computers, space vehicles, satellites and thermo-photovoltaic systems. Many techniques have been used to enhance convective heat transfer. More recent studies will be briefly discussed in the present literature review. The effect of nozzle aspect ratio on stagnation region heat transfer characteristics of elliptic impinging jet was understood by [1]. Where; the local heat transfer characteristics of an elliptic impinging jet on a heated flat plate were experimentally investigated for various nozzle aspect ratios. The flow structure was visualized using a smoke-wire technique to get a better understanding of the impinging of an elliptic jet. The stagnation point Nusselt number was correlated for the nozzle aspect ratio and the nozzle-to-plate spacing. Numerical approach for the effect of hole geometry on the film cooling effectiveness over a flat plate including internal impingement cooling chamber was done by [2]. Where; the geometrical shapes of the cooling holes are cylindrical round, simple angle (CYSA), forward-diffused, simple angle, (FDSA) and laterally diffused, simple angle (LDSA). The LDSA shape had been shown the highest value in the distribution of span wise-averaged film cooling effectiveness. Heat transfer for a jet impingement onto a plate with two-dimple configurations, (in-line and staggered) with respect to the jet impingement axis, was compared by [3]. The effect of dimple depth had also been investigated. Results indicate that the presence of dimples produces lower heat transfer coefficients rather than the plain surface. Also, it is clearly evident that the deeper dimples provide higher heat transfer coefficients for both configurations. Jet impingement, emerging from a conical nozzle, onto a cylindrical cavity has been studied numerically by [4]. Where; the influences of nozzle geometric configurations, cavity diameter and depth, on the flow structure and heat transfer rates from the cavity were investigated. A cylindrical cavity with varying diameter and depth is accommodated in the simulations. Air is used as assisting gas while steel is employed as work piece material. It is found that the flow structure changes significantly for large diameter cavity. The influence of the nozzle cone angle on the heat transfer and flow structure is more pronounced as the cavity depth increases. The Jet impingement onto a conical hole in relation to laser machining was investigated numerically by [5]. Steel was employed in the simulations as a work piece and air was introduced as an assisting gas, impinging onto the work piece surface coaxially. A numerical method using a control volume approach was introduced to solve continuity, momentum and energy equations. It was found that; the temperature profiles decayed gradually in the cavity for deep cavities. Nusselt number increases gradually in the radial direction towards the cavity exit for deep cavities. Experiments were conducted to determine the effect of the parameters that were crucial in the cooling of a heated flat plate by an obliquely impinging slot jet, [6]. The inclinations of the jet relative to the plate were (90°, 60°, 45° and 30°), for Reynolds number of 5860, 8879, and 11606. Correlations for local temperatures in terms of Reynolds number, location and inclination angle were deduced, and as a consequence, the region of maximum heat transfer (minimum temperature) on the plate could been stated with respect to the geometrical impingement axis. The heat transfer characteristics from a circular cylinder exposed to a slot air jet impingement had been studied experimentally by [7], for Reynolds

number (based on cylinder diameter) in the range of 600 up to 8000, for a cylinder diameter-to-nozzle width ratios of 0.66, 1.0 and 2.0, and for a range of distance between nozzle exit and cylinder forward stagnation point-to-nozzle width from 1 to11. The results reveal that the slot jet yields considerably higher average heat transfer than that of the parallel flow case for the same average velocity. An experimental and numerical study was carried out to investigate the flow field of a jet issuing up and impinging the down face of a horizontal surface. The velocity, turbulence intensity and pressure distribution in the impingement region were obtained for Reynolds numbers ranging from 30,000 to 50,000 and a nozzle-to-surface spacing range of 0.2–6, [8]. A sub atmospheric region occurs on the impingement surface and it moves radially outward from the stagnation point with increasing nozzle-to-surface spacing. Also, the linkage among the sub atmospheric region, turbulence intensity and heat transfer coefficients was clarified. An eight-by-eight jet array impinging onto a plate having a staggered array of dimples at Reynolds number 11,500 and spacing between the perforated plate and the target plate of 2, 4 and 8 jet diameter was investigated experimentally by [9]. Two dimple geometries of hemispherical and cusped elliptical were examined. Since the jet impingement on dimples caused a recirculation inside the dimples, the heat transfer was higher than the plain surface. The effect of dimple geometry showed that hemispherical and a cusped elliptical are not having an immensely difference. Local and average heat transfer of a row of impinging jets upon a heated-thin-foil was optimized. The influences of the impingement distance, the injection Reynolds number and the span wise spacing between jets were investigated. The measurements pointed out an optimum impingement distance (maximum heat transfer rates) within the range of about three times the nozzle diameter. An optimum span wise spacing of about five times the nozzle diameter was also recommended, [10].

In the present work, the cooling characteristics from a partially hollow finned plate due to its exposure to an air jet impingement are experimentally and numerically investigated. The finned plate heat sink of the PC processor is selected to be the test specimen. It was centrally evacuated by an adequate CNC machining to form the hollow shapes as cylindrical and frustum-conical with different vertex angles. A three-dimensional numerical model using the CFD FLUENT-6.2- code was conducted to highlight the thermo-fluid patterns of the flow field at different locations. The numerical results were validated against the experimental data. The effects of Reynolds number, angle of attack, vertex angle and nozzle-to-surface distance on the cooling characteristics were clarified. General correlations of Nusselt number versus the different parameters are also points of interest.

EXPERIMENTAL TEST RIG

A schematic diagram of the experimental apparatus is shown in figure (1). Air was supplied from a compressor and it passes through a filter. The air flow rate was measured by an orifice flow meter fitted via a straight pipe of 26.15 *mm* diameter, to issue from a nozzle. The orifice plate was designed and manufactured according to the BSI catalog data, [11]. The differential pressure head through the orifice was recorded by using a digital micro manometer having a resolution of 0.01 *mm* water. An electric

heater was installed through the straight pipe to adjust the air temperature issuing from the nozzle to be maintained at about $30^{o}C$. The test specimens that have the central hollow shapes were selected initially to be the heat sink of a PC; each one has the specifications that are given in figure (2). Six similar ones were selected initially. Five ones were centrally cut by using the wire-cut JSEDM machining, [12]. The central hollow shapes resulted from the cutting are a cylinder and four frustum cones having the same depth, *H*; as shown in figures (3) and (4). Thus, six test specimens were peppered. The specimen was heated at its bottom side of its base by a nickel-chrome heater placed between two mica layers and it gave a heat flux of about 10 kW/m^2 or more at the bottom side area of the specimen base. An asbestos layer of 10 *mm* thick was inserted between the heater and the stand. The stand and the specimen assembly allow a tilting of the specimen in increments of 15^{o} from the horizontal position, [13]. Referring to figure (5), a definite number of pre-calibrated *K*-type thermocouples of 0.1 *mm* wire diameter and of 0.02 s*econd* response time, [14] were used to measure the temperature at definite locations. Twelve locations are on the surface of the fin which coincides on *x*-axis, and other six ones are on the surface of the fin which coincides on *z*-axis. Two thermocouples were used to measure the surrounding air temperature, two ones were located bellow the heater to measure the temperature of the top side of the asbestos layer and other two ones were used to measure the temperature of the bottom side of the asbestos layer. One thermocouple measures the air temperature just before the orifice and another one measures the temperature of the air issuing from the nozzle. The experimental test rig was provided with a PC, a data acquisition system and the necessary attachments to measure temperatures at a sample time of 2.0 *seconds*, via multi I/O digital card. A PC-based data acquisition system utilizing PLC-818PG and a data logger was used for data collection and slow or rapid data monitoring, [14, 15]. The thermocouples were connected to a data acquisition system through two multiplexers (multiplexer 4051) via buffers and amplifiers. A QBasic language software program was prepared to control the data collection and monitoring. This package gives a resolution of $0.01\,^{o}C$ for temperature measurement.

EXPERIMENTAL DATA REDUCTION

The focal point of the present work is the cooling characteristics of partially hollow finned plate heat sink exposed to jet impingement. Six specimens were prepared for this purpose. Each one was heated at the bottom side of its base by an electric heater reflected from the heat form the PC processor. The amount of heat from the heater is maintained constant during all experiments as well as the air flow rate. Thus; the total heat from the heater is:

$$\dot{Q}_{\mathrm{T}} = V \times I \tag{1}$$

A small amount of the generated heat from the heater was lost by conduction through the asbestos layer which was estimated to be about 3.5%. The reminder of the total heat will be transferred to the air by convection and radiation; thus:

$$\dot{Q}_{\mathrm{conv}} = \dot{Q}_{\mathrm{T}} - \dot{Q}_{\mathrm{cond,\ ins}} - \dot{Q}_{\mathrm{rad}} \tag{2}$$

Referring to the shown scheme of the fins geometry, the heat loss by radiation and as a consequence the convective heat transfer can be found at fins root, mid-plane and tip as follows, [16 and 17]:

$$\varepsilon_c = \frac{\dfrac{\varepsilon A_b \left(A_f + A_{f,o} + A_{b,c}\right)}{\left[A_{b,c} + \varepsilon(A_f + A_{f,o})\right]} + \varepsilon A_t}{A_{b,c} + A_t} \tag{3}$$

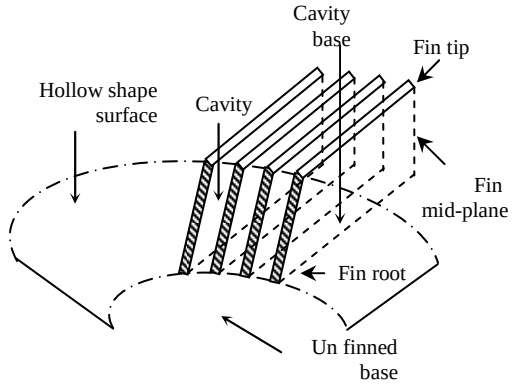

$$Q_{\text{rad}} = \sigma(A_{b,c})\varepsilon_c(T_{b,c}^4 - T_a^4) + \sigma(A_t)\varepsilon(T_t^4 - T_a^4)$$

$$\frac{\sigma A_f (T_f^4 - T_{f,o}^4)}{\dfrac{A_f + A_{f,o} - 2A_f F}{A_{f,o} - A_f (F)^2} + \left(\dfrac{\varepsilon - 1}{\varepsilon}\right)\left(\dfrac{A_f + A_{f,o}}{A_{f,o}}\right)} \tag{4}$$

$$Q_{\text{cond, b}\to r} = \frac{A_b \times (T_b - T_r)}{(\delta_b / k_s)} \tag{5}$$

$$Q_{\text{cond, r}\to \text{m}} = \frac{2 \times a \times (T_r - T_m)}{(H / k_s)} \tag{6}$$

$$Q_{\text{cond, m}\to t} = \frac{2 \times a \times (T_m - T_t)}{(H / k_s)} \tag{7}$$

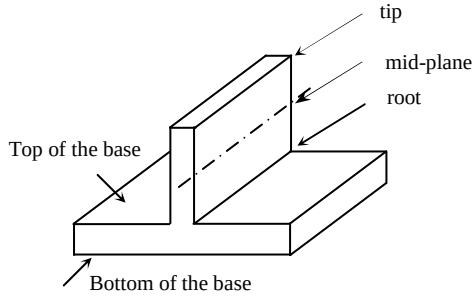

$$\begin{aligned} Q_{\text{conv}} &= Q_{\text{conv, }(b,c)} + Q_{\text{conv, }(f)} \\ &= A_{b,c} h_{b,c} (T_{b,c} - T_a) + \frac{A_f}{2} h_r (T_r - T_a) + \frac{A_f}{2} h_m (T_m - T_a) + A_t\ h_t (T_t - T_a) \end{aligned} \tag{8}$$

From the earlier equations; one can get the convective heat transfer from the lower and upper half areas of the fin as well as the fin tip, and consequently Nusselt number can be found at fins root, mid plane and tip as follows:

$$Nu_r = \frac{h_r \times d_n}{k_a} \tag{9}$$

$$Nu_m = \frac{h_m \times d_n}{k_a} \tag{10}$$

$$Nu_t = \frac{h_t \times d_n}{k_a} \tag{11}$$

In this data reduction, the enhancement ratio is due to the central cut of hollow shapes, the angle of attack and the nozzle-to-surface distance. Thus the enhancement ratio is given as follows:

The enhancement ratio (due to hollow shapes); $\xi_g = \dfrac{Nu\big|_{\text{with hollow shapes}}}{Nu\big|_{\text{without hollow shapes}}}$ (12)

The enhancement ratio (due to angle of attack); $\xi_\theta = \dfrac{Nu\big|_{\text{with } \theta \neq 0}}{Nu\big|_{\text{with } \theta = 0}}$ (13)

The enhancement ratio (due to nozzle-to-surface distance);

$$\xi_y = \frac{Nu\big|_{\text{with } (y/d_n \neq 0)}}{Nu\big|_{\text{with } (y/d_n = 0)}} \tag{14}$$

NUMERICAL MODEL

The governing equations that describe the thermo fluid characteristics through the finned plate are a set of non-linear partial differential equations. The air flow is governed by the mass, momentum and energy equations. Generally, the governing equations can be written as [18]:

Continuity equation; $\dfrac{\partial \rho}{\partial t} + div\ (\rho \mathbf{u}) = 0$ (15)

Momentum equations;

$$\frac{\partial(\rho u)}{\partial t} + div\,(\rho u\ \mathbf{u}) = -\frac{\partial p}{\partial x} + div\ (\mu\ grad\ u) - \left[\frac{\partial(\rho\overline{u'^2})}{\partial x} + \frac{\partial(\rho\overline{u'v'})}{\partial y} + \frac{\partial(\rho\overline{u'w'})}{\partial z}\right] \tag{16}$$

$$\frac{\partial(\rho v)}{\partial t} + div\,(\rho v\ \mathbf{u}) = -\frac{\partial p}{\partial y} + div\,(\mu\ grad\ v) - \left[\frac{\partial(\rho\overline{u'v'})}{\partial x} + \frac{\partial(\rho\overline{v'^2})}{\partial y} + \frac{\partial(\rho\overline{v'w'})}{\partial z}\right] \tag{17}$$

$$\frac{\partial(\rho w)}{\partial t} + div\,(\rho w\ \mathbf{u}) = -\frac{\partial p}{\partial z} + div\,(\mu\ grad\ w) - \left[\frac{\partial(\rho\overline{u'w'})}{\partial x} + \frac{\partial(\rho\overline{v'w'})}{\partial y} + \frac{\partial(\rho\overline{w'^2})}{\partial z}\right] \tag{18}$$

Energy equation;

$$\frac{\partial(\rho E)}{\partial t} + div\,(\rho E\ \mathbf{u}) = div\,(k\ \ grad\ T) - \left[\frac{\partial(\rho\overline{u'E'})}{\partial x} + \frac{\partial(\rho\overline{v'E'})}{\partial y} + \frac{\partial(\rho\overline{w'E'})}{\partial z}\right] \tag{19}$$

Heat conduction equation; $\dfrac{\partial T}{\partial t} = \alpha \nabla^2 T$ (20)

The boundary conditions for the numerical model were taken to be as symmetrical conditions specified at the planes that intersect at the jet axis. At the upstream boundary, a uniform flow with a velocity u_j and a temperature T_j was specified. At the downstream end which is located at 20 *mm* from the fin side tip, pressure was set to atmospheric pressure (zero gauge). At the symmetry planes, all normal components and their gradients were set to be zeros. At the top side surface of the base, no-slip conditions and a constant heat flux was specified. The solving of the heat transfer through the fin was solved by the coupling of both conduction and convection equations.

In order to solve these equations, a finite volume discretization method using a SIMPLE-based solution algorithm of the velocity-pressure coupling is applied with a segregated solver. The numerical modeling of the turbulent flow through the finned plate is solved using FLUENT-6.2.16 CFD program. The momentum and energy equations are solved by the second order upwind scheme. The thermo fluid

characteristics from the finned plate is treated using *k-ε* RNG "renormalization group" turbulence model. The RNG model is more accurate and reliable for a wider class of flow than the standard *k-ε* model, [19].

The transport equations of the RNG *k-ε* model are given as;

$$\frac{\partial}{\partial t}(\rho k)+\frac{\partial}{\partial x_i}(\rho k u_i)=\frac{\partial}{\partial x_j}\left(\alpha_k \mu_{eff}\frac{\partial k}{\partial x_j}\right)+G_k+G_b-\rho\varepsilon+S_k \quad (21)$$

$$\frac{\partial}{\partial t}(\rho \varepsilon)+\frac{\partial}{\partial x_i}(\rho \varepsilon u_i)=\frac{\partial}{\partial x_j}\left(\alpha_\varepsilon \mu_{eff}\frac{\partial \varepsilon}{\partial x_j}\right)+C_{1\varepsilon}\frac{\varepsilon}{k}(G_k+C_{3\varepsilon}G_b)-C_{2\varepsilon}\rho\frac{\varepsilon^2}{k}-R_\varepsilon+S_k \quad (22)$$

Where;

$$G_k=-\rho\overline{u_i' u_j'}\frac{\partial u_j}{\partial x_i},\ G_b=g_i\frac{\mu_t}{\rho Pr_t}\frac{\partial \rho}{\partial x_i},\ S_k=\zeta\varepsilon,\ C_{1\varepsilon}=1.42,\ C_{2\varepsilon}=1.42,$$

$$C_{3\varepsilon}=\tanh\left|\frac{v}{u}\right|,\ R_\varepsilon=\frac{C_\mu\rho\zeta^3\left(1-\zeta/\zeta_0\right)}{1+\psi\zeta^3}\frac{\varepsilon^2}{k},\ \zeta=4.34,\ \alpha_k=\alpha_\varepsilon\approx 1.393,$$

and $\psi=0.012$.

The term G_k represents the generation of turbulence kinetic energy due to the mean velocity gradients and G_b represents the generation of turbulence kinetic energy due to buoyancy. The quantities α_k and α_ε are the inverse of Prandtl numbers for both *k* and ε respectively, [20]. The numerical solution transforms the partial differential equations into algebraic forms and solves them to obtain a set of flow field values at discrete points of time and space

RESULTS AND DISCUSSION

In the vision of the previous analysis, the experimental results were reduced and plotted as non-dimensional quantities. A comparative study was presented for a constant heat flux of $9\,kW/m^2$ at the bottom side of the base and at a constant air flow rate. Three nozzles were used of diameters, 1.5, 2.5 and 3.5 *mm*, respectively. The six test-specimens with their different configurations were tested at almost the same boundary conditions. For the specimen I, which the heat sink of the PC, a comparison among Nusselt number versus the specimen length at fins tip, mid-plane and fins root is shown in figure (6). Also, another comparison among Nusselt number versus the specimen width at fins tip, mid-plane and fins root is shown in figure (7). The values of Nusselt numbers in the two figures (6 and 7) were taken as reference values to state how much the cutting of central holes enhances the cooling characteristics. Figures (8 and 9), show comparison among enhancement ratio ξ_g at fins tip versus length *x* and width z, respectively, for the six specimens, for $y/d_n=10$, $\mathrm{Re}=55674$ and $\theta=0^o$. From the given data of figures (6-9), one can obtain the enhancement ratio of the cooling characteristics to be tabulated as follows:

At fins tip:

Specimen No.	I	II	III	IV	V	VI
Enhancement ratio, ξ_g	0%	12.5%	25%	30.8%	35%	38.3%

Figures (10 and 11), show comparison among ξ_g at fins mid-plane versus length *x* and width y for the six test-specimens, for $y/d_n = 10$, $\mathrm{Re} = 55674$ and $\theta = 0^o$. From these data and reference data of the specimen No. I, one can find:

At fins mid-plane:

Specimen No.	I	II	III	IV	V	VI
Enhancement ratio, ξ_g	0%	16.3%	32.5%	40%	45%	48.8%

Figures (12 and 13), show comparison among ξ_g at fins root versus length *x* and width y for the six test-specimens, for $y/d_n = 10$, $\mathrm{Re} = 55674$ and $\theta = 0^o$. From these data and reference data of the specimen No. I, one can find:

At fins root:

Specimen No.	I	II	III	IV	V	VI
Enhancement ratio, ξ_g	0%	18.5%	41.5%	60.1%	69.2%	76.9%

When the test specimen was tilted by an angle θ; the maximum value of Nusselt number moves from the center of the specimen towards a location which is divided the specimen along its length into two zones; uphill-zone and down-hill zone, [21]. The air issue from the nozzle is near enough to the uphill-zone. Referring to figures (14-16), one can notice at the fins tip; for $\theta = 30^o$ the uphill-zone lays at $-0.5 \le x/L \le -0.303$; for $\theta = 45^o$ the uphill-zone lays at $-0.5 \le x/L \le -0.401$ and for $\theta = 60^o$ the uphill-zone concentrates at $x/L = -0.5$. Referring to figures (17-22), one can state at the fins mid-plane and fins root where the uphill-zone lays as those at the fins tip. From these results, it is evident that the enhancement ratio of cooling characteristics at uphill-zones may be $16\% \le \xi_\theta \le 100\%$.

Figure (23) shows a comparison among enhancement ratio versus length *x* for the test-specimen No. VI, for positive, zero and negative values of nozzle-to-surface spacing, y/d_n at Reynolds number, $\mathrm{Re} = 55674$ and zero angle of attack, $\theta = 0^o$. As the nozzle-to-surface distance y/d_n decreases to be a negative value, It occurs an accumulation of air at fins root and fins mid-plane to form a stagnation zone at fins-root and hence the air flow reverses up as the so-called hydraulic jump and flowed beyond the jump as a tranquil streaming regime between the fins, [22 and 23]. From this point, one may imply the following quantitative cooling enhancement for considering $y/d_n = 0$ as a reference value;

y/d_n	10			0			-10		
Location	Tip	Mid-plane	Root	Tip	Mid-plane	Root	Tip	Mid-plane	Root
Enhancement ratio, ξ_y %	-13.1	-20	-21.8	0	0	0	12.8	16.2	23.5

The three dimensional numerical solution yields the flow pattern as shown in figure (24). Figure (24-a) exhibits the constant temperature contours in the *x-y* plane for the two-dimensional solution of the numerical model. The same trend was noticed for the two planes *x-y* and *z-y* planes for the three dimensional solution of the numerical model as shown in figure (24-b). Figure (24-c) gives the velocity contours for the three-dimensional solution. From these figures, it is noting that a recirculation flow characteristics can be formed depending on the flow source. It is clear that the free jet behaves more ax-symmetric along y-axis up to the stagnation area at the specimen base, and hence, air jumps up as the hydraulic jump which is seen for water flowed under sluice gates. After this jump air flows as some what tranquil quiet stream parallel to the fins area. The isothermal contours of air and solid at three horizontal levels; fins tip, fins mid-plane and fins root are shown in figure (24-d). The figure shows a high temperature of air at the stagnant layer at the fins root. The numerical model reduces also the contours of the local values of Nusselt number. It was plotted for one quadrant of the specimen at three horizontal levels; fins tip, fins mid-plane and fins tip as shown in figure (25). The fins print is clear in this figure and a reasonable low value of Nusselt number was found at the stagnant area at the root level.

COMPARISON AMONG PRESENT WORK AND PREVIOUS ONES

Figure (26) gives a comparison among the results of both present experimental work and numerical CFD one as well as the previous work given by [10, 24 and 25]. Referring to this figure, a well established agreement between present experimental and CFD results is obvious with ±10% or less. Local heat transfer of a row of impinging jets upon a heated-thin-plate was optimized by [10]. The measurements optimize the impingement distance to be of about three times the nozzle diameter. An optimum span wise spacing of about five times the nozzle diameter was also recommended. The effect of jet-to-jet spacing of five staggered circular jets onto a heated flat plate was studied and correlated experimentally by [24]. The correlation involves Reynolds number, jet-to-jet spacing and jet-to-surface distance to give the local Nusselt number on the heated plate. A comparative CFD study of heat transfer of a turbulent slot jet onto a flat surface was carried out using five low Reynolds number $k-\varepsilon$ models was done by [25]. The predicted local Nusselt number distributions were found. Both experimental data of [10 and 24] were carried out from a jet impingement onto a flat surface, also, the CFD data of [25] was carried out from a jet impingement onto a flat surface. These data were plotted with both experimental and CFD data of the present work to show that the Nusselt number of the present work is less than those

of the literature. However; the finned surface of the present work has more surface area to sustain more thermal cooling rather than those of the literature.

CONCLUSIONS

In the present work, the cooling characteristics of partially hollow finned plate due to its exposure to jet impingement were experimentally and numerically investigated. Six test specimens were manufactured with particular reference of the heat sink of the PC processor. The effects of jet flow rate, angle of attack and nozzle-to-surface distance on the cooling characteristics have been verified. Numerical CFD investigation using finite volume method was conducted to predict the model performance extensively. The validated CFD model was extended to view the flow characteristics through the specimens. The main concluded data from this work are:

1. The cutting of the middle of the heat sink of a PC to form cylindrical and frustum-conical hollow shapes will enhance the heat transfer by about 40% at fins tip, about 50% at fins mid-plane and about 80% at fins root rather than the non-cut heat sink if both were exposed to jet impingement of air at the same test conditions.
2. Hollow shapes foundations with certain geometry in the heat sinks will save some amount of material and reduce the weight.
3. The negative values of jet-to-specimen spacing enhance the cooling characteristics at fins tip by about 13%, and by about 16% at fins mid-plane and by about 24% at fins tip.
4. The proposed CFD model can be employed to simulate other configurations rather than that were presented in the present work.
5. The experimental results can be summarized as following:

$$Nu_{\max,\,t} = 0.04\, Re^{0.471}\,(1+0.782\tan\beta)\left|\left(\frac{y}{d_n}\right)^{0.013}\right|$$

$$Nu_{\max,\,m} = 0.04\, Re^{0.471}\,(1+0.982\tan\beta)\left|\left(\frac{y}{d_n}\right)^{0.013}\right| \qquad \text{For} \begin{cases} 25146 \le \mathrm{Re} \le 58674 \\ 0 \le \beta \le 42.8^0 \\ -10 \le \dfrac{y}{d_n} \le 10 \end{cases} \qquad (23)$$

$$Nu_{\max,\,r} = 0.04\, Re^{0.471}\,(1+1.975\tan\beta)\left|\left(\frac{y}{d_n}\right)^{0.013}\right|$$

REFRENCES

[1] Lee, J. and Lee, S., (2000), *the Effect of Nozzle Aspect Ratio on Stagnation Region Heat Transfer Characteristics of Elliptic Impinging Jet*, International Journal of Heat and Mass Transfer (43), pp. 555-575.

[2] Miao, J. and Wu, C., (2006), *Numerical Approach to Hole Shape Effect on Film Cooling Effectiveness over Flat Plate Including Internal Impingement Cooling Chamber*, International Journal of Heat and Mass Transfer (49), pp. 919–938.

[3] Ekkad, S.V. and Kontrovitz, D., (2002), *Jet Impingement Heat Transfer on Dimpled Target Surfaces*, International Journal of Heat and Fluid Flow (23), pp. 22–28.

[4] Shuja, S.Z., Yilbas, B.S. and Budair, M.O., (2007), *Jet Impingement on Cylindrical Cavity: Conical Nozzle Considerations*, Journal of Fluids and Structures (23), pp. 1106–1118.

[5] Yilbas, B.S., Shuja, S.Z. and Budair, M.O. , (2004), *Jet Impingement onto a Conical Hole in Relation to Laser Machining*, Journal of Materials Processing Technology 155–156, pp. 2039–2044

[6] Eren, H. and Celik, N., (2006), *Cooling of a Heated Flat Plate by an Obliquely Impinging Slot Jet*, International Communications in Heat and Mass Transfer (33), pp. 372–380.

[7] McDaniel, C.S. and Webb, B.W., (2000), *Slot Jet Impingement Heat Transfer from Circular Cylinders, International Journal of Heat and Mass Transfer* (43), pp. 1975-1985.

[8] Baydar, E. and Ozmen, Y., (2005), *An Experimental and Numerical Investigation on a Confined Impinging Air Jet at High Reynolds Numbers*, Applied Thermal Engineering (25), pp. 409–421.

[9] [9] Kanokjaruvijit, K. and Martinez-botas, R.F., (2005), *Jet Impingement on a Dimpled Surface with Different Cross Flow Schemes*, International Journal of Heat and Mass Transfer (48), pp. 161–170.

[10] Brevet, P., Dejeu, C., Dorignac, E., Jolly, M. and Vullierme, J.J, (2002), *Heat Transfer to a Row of Impinging Jets in Consideration of Optimization*, International Journal of Heat and Mass Transfer (45), pp. 4191–4200.

[11] BSI, (1981), *Methods of Measurement of Fluid Flow in Closed Conduits*, part 1, British Standards Institution, BS 1402: Section 1.1: 1981.

[12] JSEDM, *WIRECUT EDM, Operation Instruction*, Jiann Sheng Machinery & Electric Industrial Co., LTD

[13] Gomaa, A.G., Eid, E.I. and Gomaa, M.E., (2007), *An Experimental Investigation of Heat Transfer Characteristics for a Single Jet Impingement onto an Array of Thin Strips Pin Fins*, Eng. Research J., Helwan University, Faculty of Eng., Mataria, Cairo, pp M122-M141.

[14] Holman, J.P., (2001), *Experimental Methods for Engineers*, McGraw-Hill International Edition, Seventh Edition, New York, USA.

[15] Rahimi, M., Owen, I. and Mistry, J., (2003), *Impingement Heat Transfer in an Under-Expanded Axsymmetric Air Jet*, International Journal of Heat and Mass Transfer (46), pp. 263–272.

[16] Holman, J.P. (2002), *Heat Transfer*, Ninth Edition, New York, McGraw-Hill Inc.

[17] Faires, J.D and Burden, R., (1998), *Numerical Methods*, 2nd Edition, BROOKS/COLE PUBLISHING COMPANY, 511 Forest Lodge Road, Pacific Grove, CA 93950, USA.

[18] Versteeg H. K. and Malalasesekera W., (1995), *An introduction to computational fluid dynamics*, the finite volume method. Longman Group LTD, UK.

[19] Afify R., Berbish N., Gomaa A., and Eid A., (2004), *Numerical and*

Experimental Study of Turbulent Flow and Convective Heat Transfer in a Circular Tube with Disc-Baffles, Engineering research journal, Helwan University, Faculty of Eng., Vol. 96, PP. M37-M61.

[20] FLUENT, *user's manual*, Fluent Inc., USA, 2005.

[21] Beitelmal, A.H., Saad, M.A., and Patel, C.D., (2000), *The Effect of Inclination on the Heat Transfer Between a Flat Surface and an Impinging Two-Dimensional Air Jet*, Int. J. of Heat and Fluid Flow 21, pp. 156-163.

[22] Baonga, J.B., Louahlia-Gualous, H. and Imbert, M., (2006), *Experimental Study of the Hydrodynamic and Heat Transfer of Free Liquid Jet Impinging a Flat Circular Heated Disk,* Applied Thermal Engineering (26), pp. 1125–1138

[23] Angioletti, M., Nino, E. and Ruocco, G., (2005), *CFD Turbulent Modeling of Jet Impingement and its Validation by Particle mage Velocimetry and Mass Transfer Measurements*, International Journal of Thermal Sciences (44), pp. 349–356.

[24] Yang-San, J and Lai, M., (2001), *Optimum Jet-to-Jet Spacing of Heat Transfer for Staggered Arrays of Impinging Jets*, International Journal of Heat and Mass Transfer (44), pp. 3997–4007.

[25] Wang, S.G. and Mujumdar, A.S., (2005), *A Comparative Study of Five Low Reynolds Number k– ε Models for Impingement Heat Transfer*, Applied Thermal Engineering (25), pp. 31–44.

1- Compressor
2- Regulator
3- Water filter
4- Gas filter
5- Valve
6- Orifice meter
7- Digital manometer
8- Heater
9- Nozzle
10- Test specimen
11- Data cable
12- Data acquisition system
8 - PC
- Tilting stand

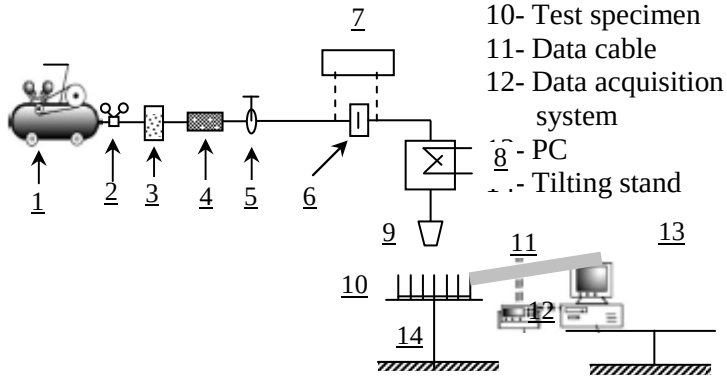

Figure (1), Experimental test rig and measuring equipments.

Number of fins = 19 fins;
Fin Length, L = 66.04 *mm*; width, W=49.4 *mm*
Fin height, H = 32.7 *mm*;
Fin thickness, δ_f = 0.8 *mm*;
Pitch, s = 2.7 *mm*;
Base thickness, δ_b = 4.1*mm*;
Material: Aluminum;
Specimen weight = 118.5 *gm*.

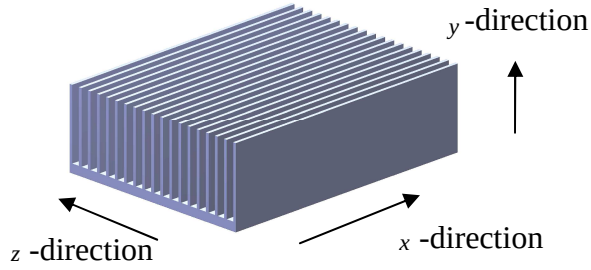

Figure (2), Test specimen before the cutting of the central holes, specimen no. I.

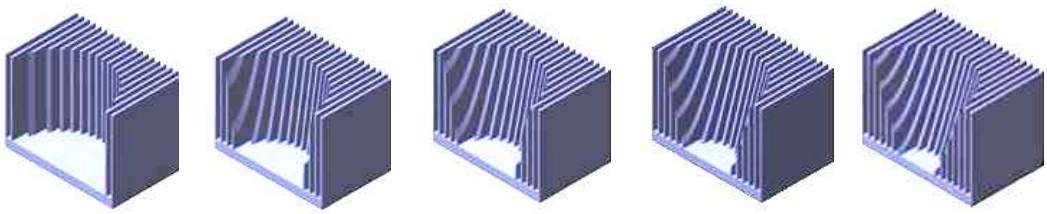

Specimen no. II Specimen no. III Specimen no. IV Specimen no. V Specimen no. VI

Figure (3), Photograph of the test specimens after the cutting of central holes.

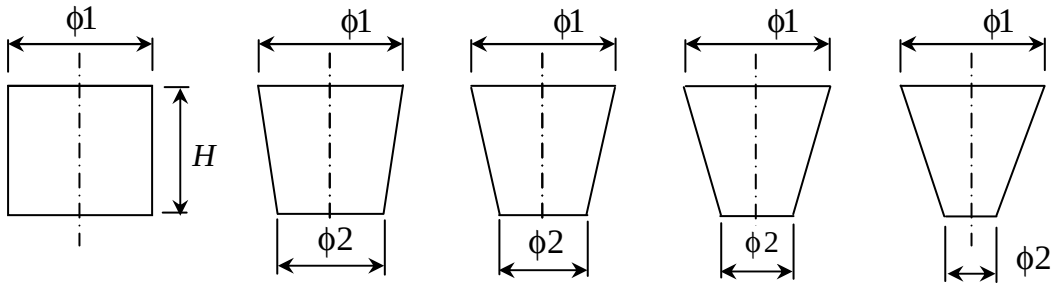

Hole in the specimen No. II
$H = 32.7\ mm$;
$\phi 1 = 40\ mm$;
$\beta 1 = 0^{o}$

Hole in the specimen No. III
$\phi 1 = 40\ mm$;
$\phi 2 = 30\ mm$;
$\beta 2 = 17.4^{o}$

Hole in the specimen No. IV
$\phi 1 = 40\ mm$;
$\phi 2 = 25\ mm$;
$\beta 3 = 25.8^{o}$

Hole in the specimen No. V
$\phi 1 = 40\ mm$;
$\phi 2 = 20\ mm$;
$\beta 4 = 34^{o}$

Hole in the specimen No. VI
$\phi 1 = 40\ mm$;
$\phi 2 = 15\ mm$;
$\beta 5 = 41.8^{o}$

Figure (4), Geometry of the central holes.

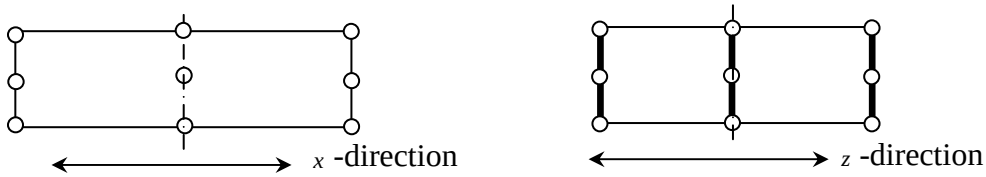

Figure (5-a), Locations of thermocouples on the surface of fins that coincide on *x* and *z* axis for the specimen having no central holes, (specimen no. I).

Figure (5-b), Locations of thermocouples on the surface of fins that coincide on *x* and *z* axis for the specimen having cylinderical central hole, (specimen no. II).

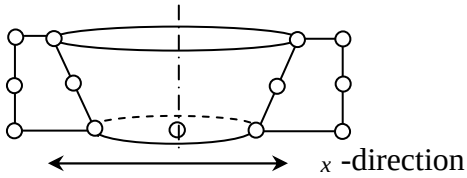

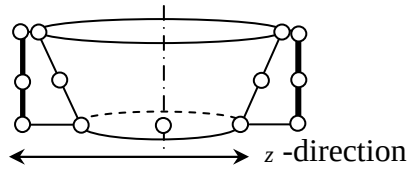

Figure (5-c), Locations of thermocouples on the surface of fins that coincide on *x* and z axis for the specimen having frustum conical central holes, (specimens no. III, IV, V and VI).

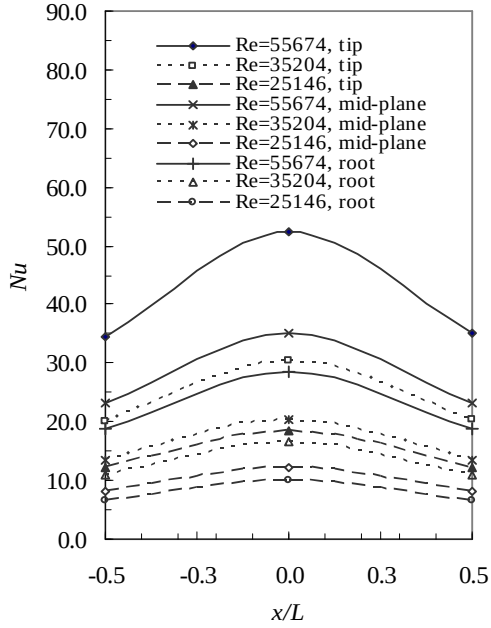

Figure (6), variation of Nusselt number versus *x* for specimen no. I, for $y/d_n = 10$ and θ=0.

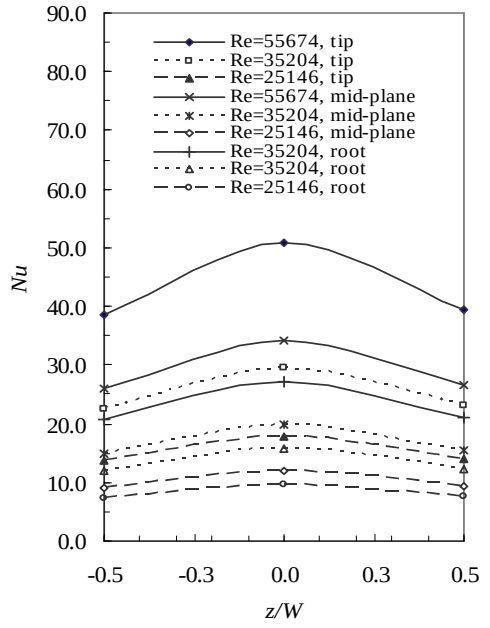

Figure (7), variation of Nusselt number versus *z* for specimen no. I, for $y/d_n = 10$ and θ=0.

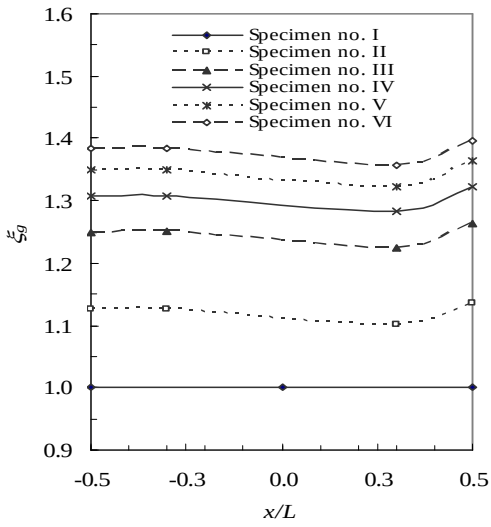

Figure (8), Comparison among enhancement ratio at fins tip versus length x for the six test-specimens, for $y/d_n = 10$, Re =55674 and θ=0.

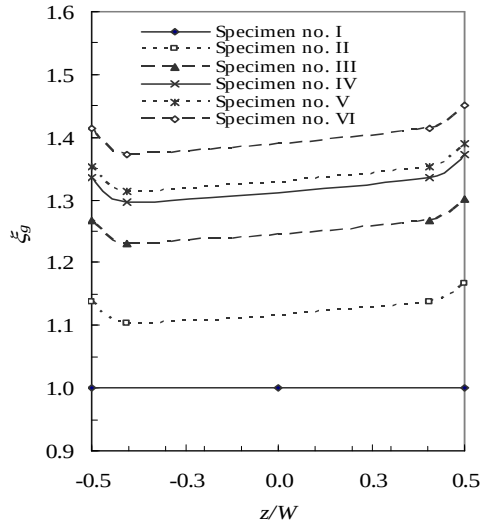

Figure (9), Comparison among enhancement ratio at fins tip along width y for the six test-specimens, for $y/d_n = 10$, Re =55674 and θ=0.

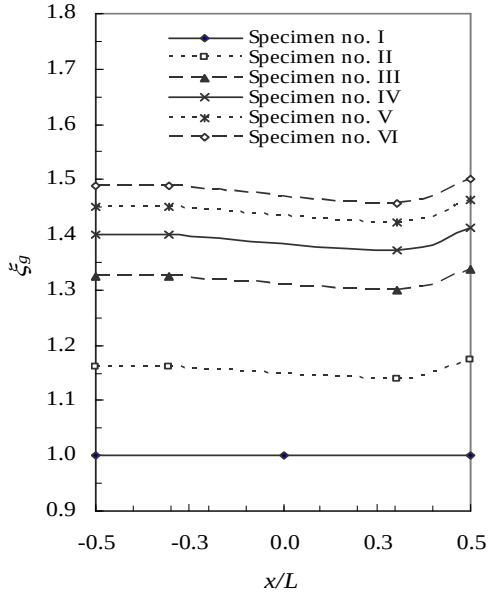

Figure (10), Comparison among enhancement ratio at fins mid-plane versus length x for the six test-specimens, for $y/d_n = 10$, Re =55674 and θ=0.

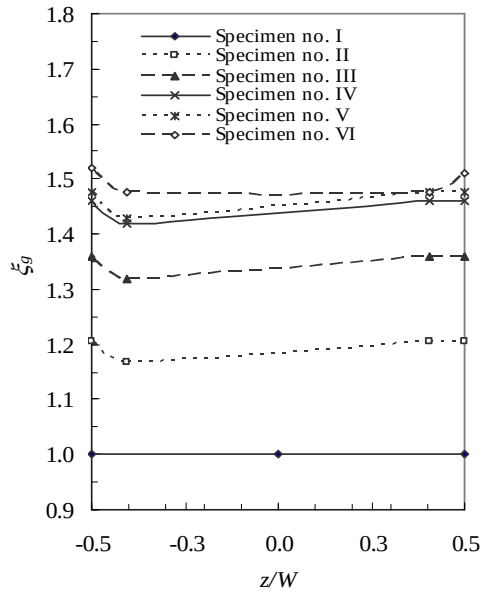

Figure (11), Comparison among enhancement ratio at fins mid-plane along y for the six test-specimens, for $y/d_n = 10$, Re =55674 and θ=0.

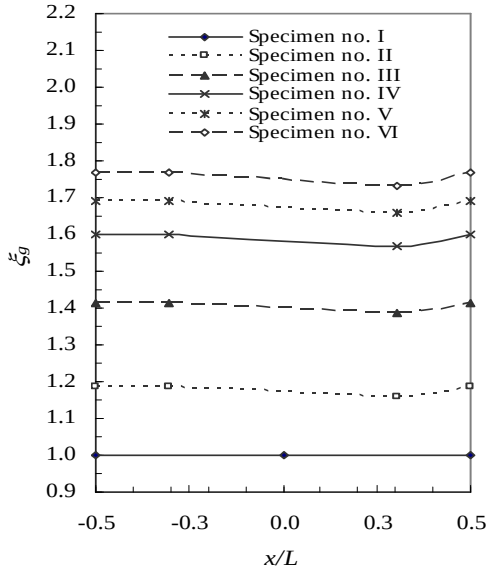

Figure (12), Comparison among enhancement ratio at fins root versus length x for the six test-specimens, for $y/d_n = 10$, Re =55674 and θ=0.

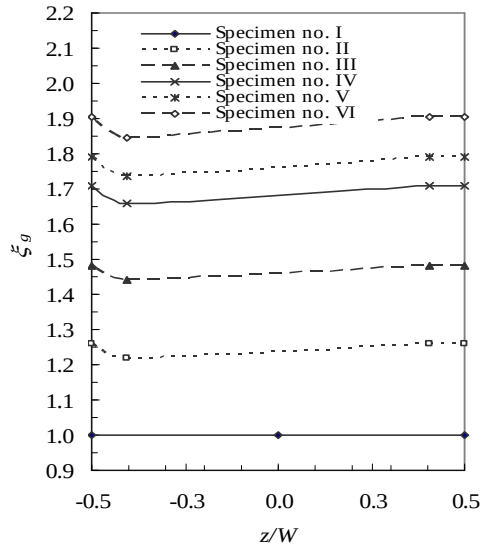

Figure (13), Comparison among enhancement ratio at fins root along width y for the test-specimens, for $y/d_n = 10$, Re =55674 and θ=0.

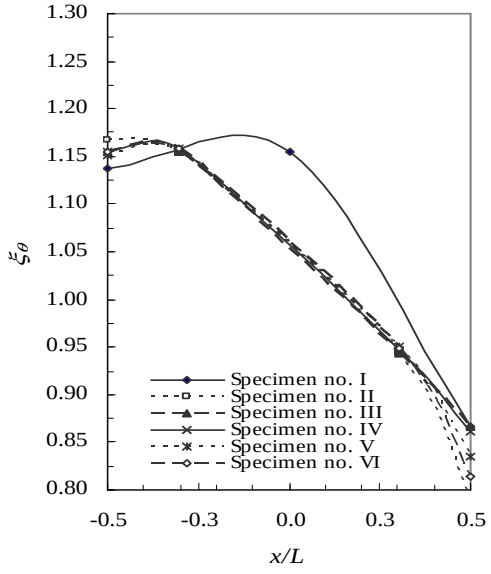

Figure (14), Comparison among enhancement ratio at fins tip versus length x for the six test-specimens, for $y/d_n = 10$, Re =55674 and θ=30^o.

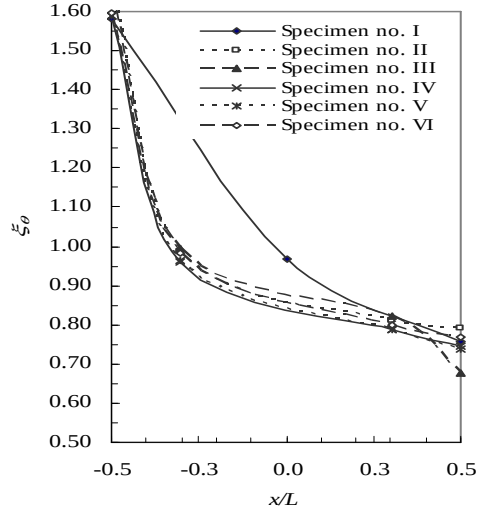

Figure (15), Comparison among enhancement ratio at fins tip versus length x for the six test-specimens, for $y/d_n = 10$, Re =55674 and θ=45^o.

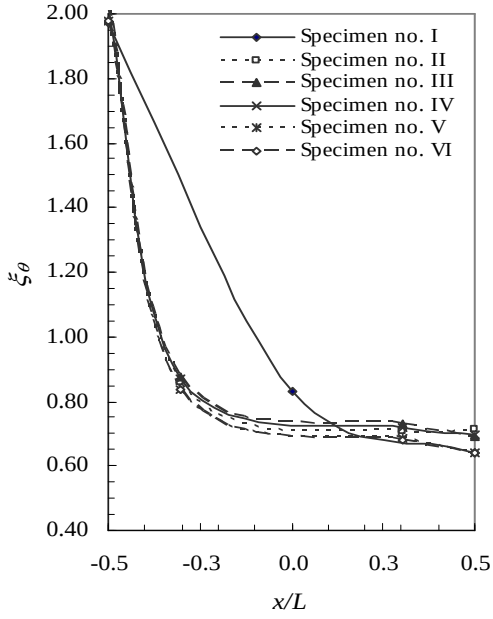

Figure (16), Comparison among enhancement ratio at fins tip versus length x for the six test-specimens, for $y/d_n = 10$, Re =55674 and θ=60°.

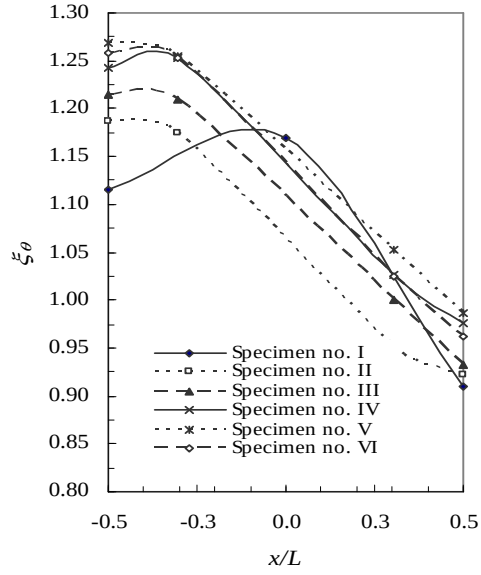

Figure (17), Comparison among enhancement ratio at fins mid-plane versus length x for the test-specimens, for $y/d_n = 10$, Re =55674 and θ=30°.

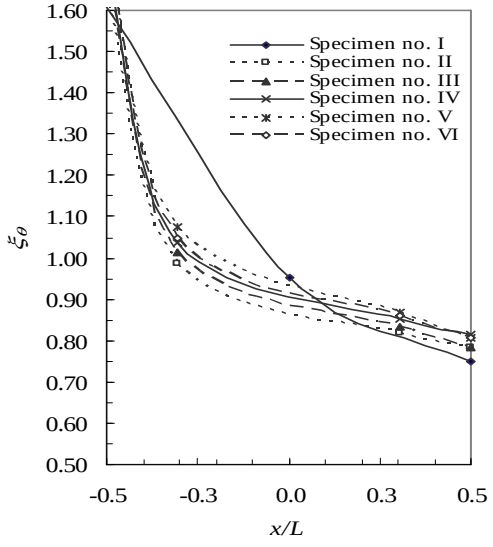

Figure (18), Comparison among enhancement ratio at fins mid-plane versus length x for the six test-specimens, for $y/d_n = 10$, Re =55674 and θ=45°.

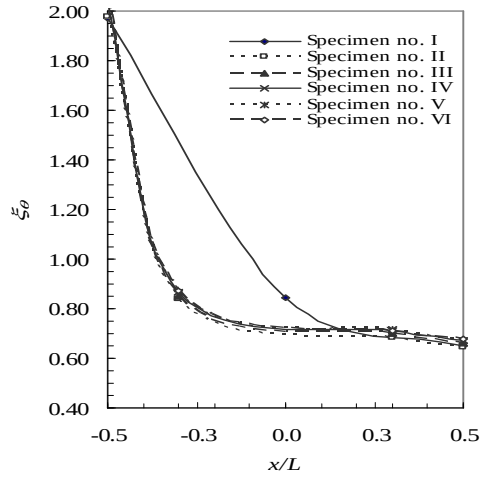

Figure (19), Comparison among enhancement ratio at fins mid-plane versus length x for the test-specimens, for $y/d_n = 10$, Re =55674 and θ=60°.

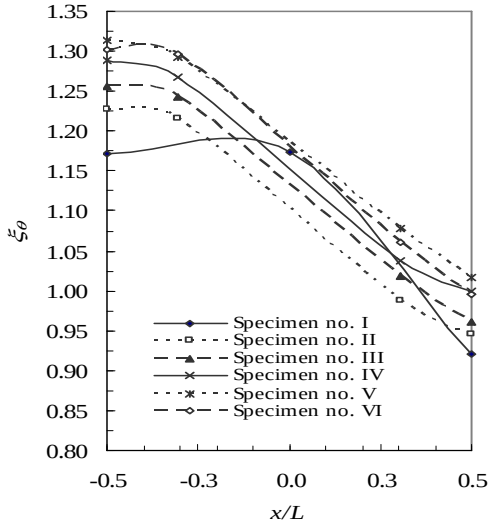

Figure (20), Comparison among enhancement ratio at fins root versus length x for the six test-specimens, for $y/d_n = 10$, Re =55674 and θ=30^o.

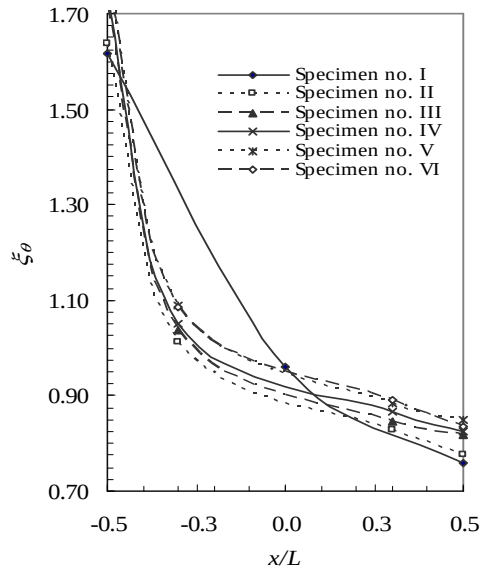

Figure (21), Comparison among enhancement ratio at fins root versus length x for the six test-specimens, for $y/d_n = 10$, Re =55674 and θ=45^o.

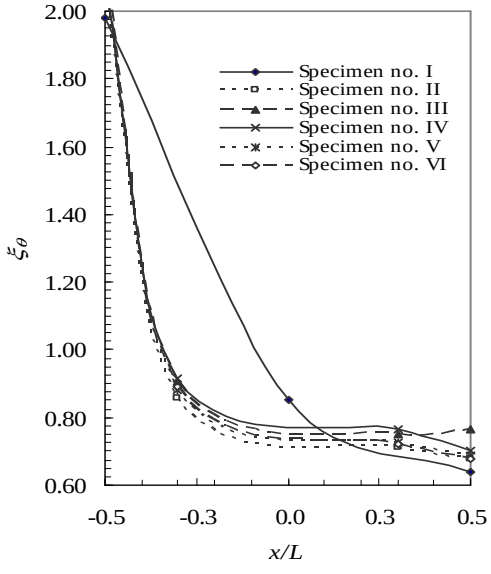

Figure (22), Comparison among enhancement ratio at fins root versus length x for the six test-specimens, for $y/d_n = 10$, Re =55674 and θ=60^o.

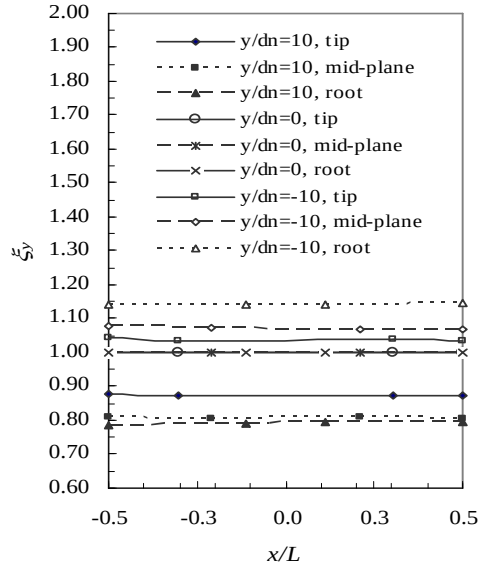

Figure (23), Comparison among enhancement ratio versus length x for the test-specimen No. VI, for different y/d_n, Re =55674 and θ=0^o.

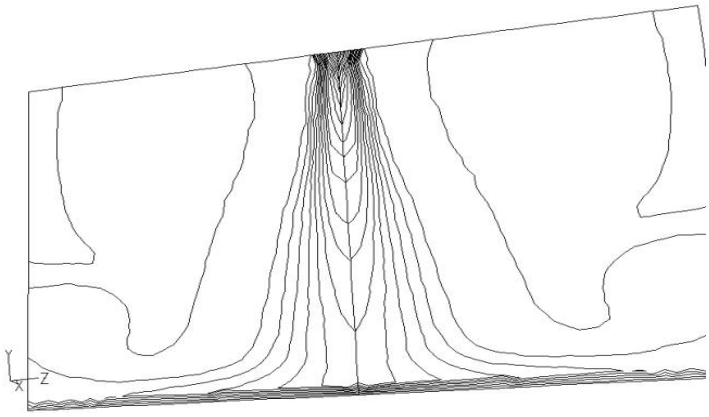

Figure (24-a) Isothermal contours of air in *x-y* plane which intersects the jet axis.

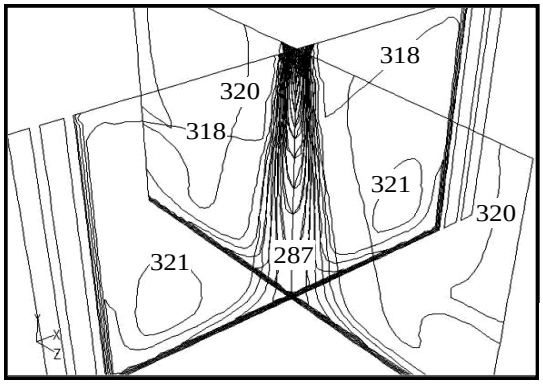

Figure (24-b), Isothermal contours in *K* of air in *x-y* and *z-y* planes that intersect at the jet-axis.

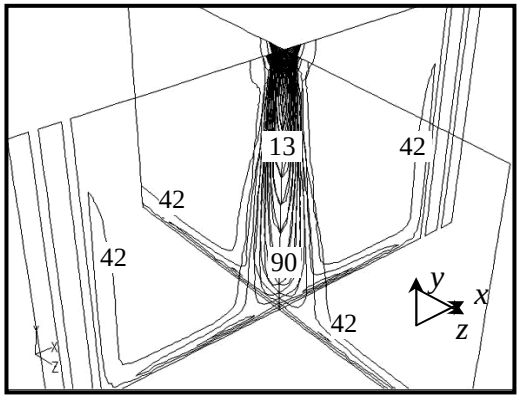

Figure (24-c), Velocity contours in *m/s* of air in *x-y* and *z-y* planes that intersect at the jet-axis.

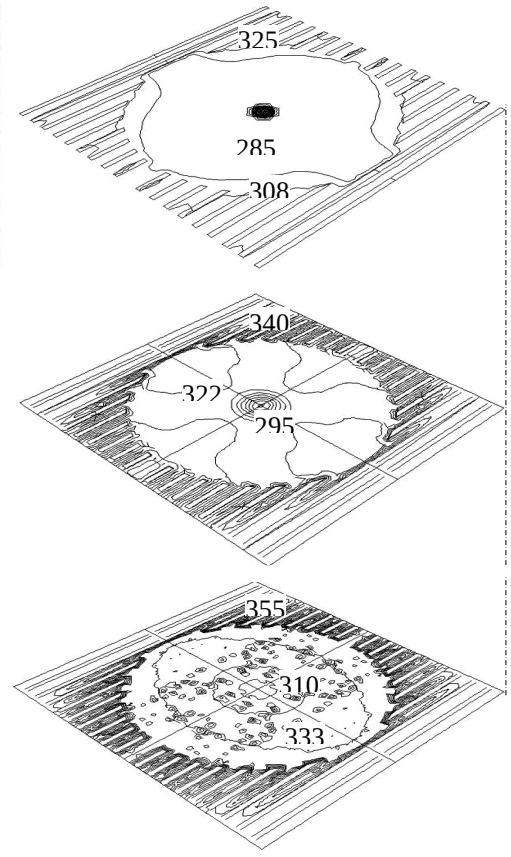

Figure (24-d), Isothermal contours of air at fins tip, fins mid-plane and fins root.

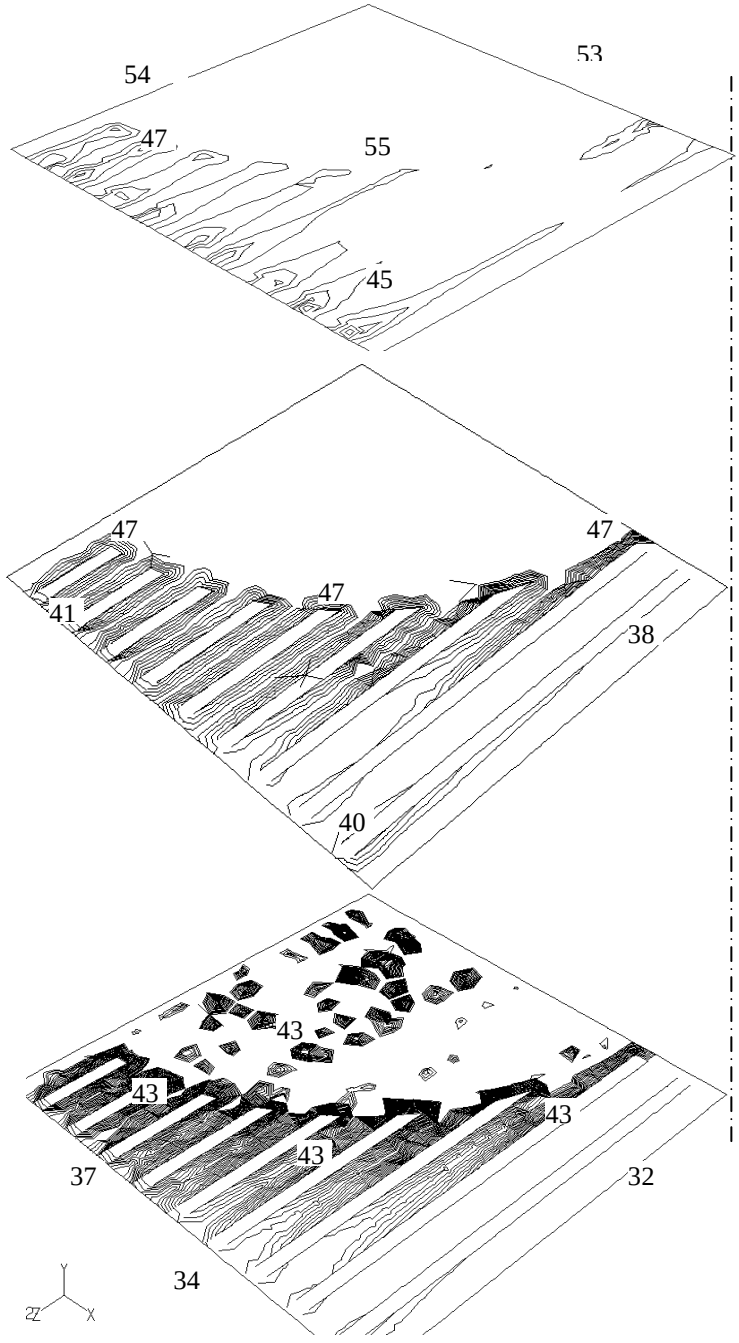

Figure (25), Contours of local Nusselt number for specimen No. II, for $y/d_n = 10$ and θ=0.

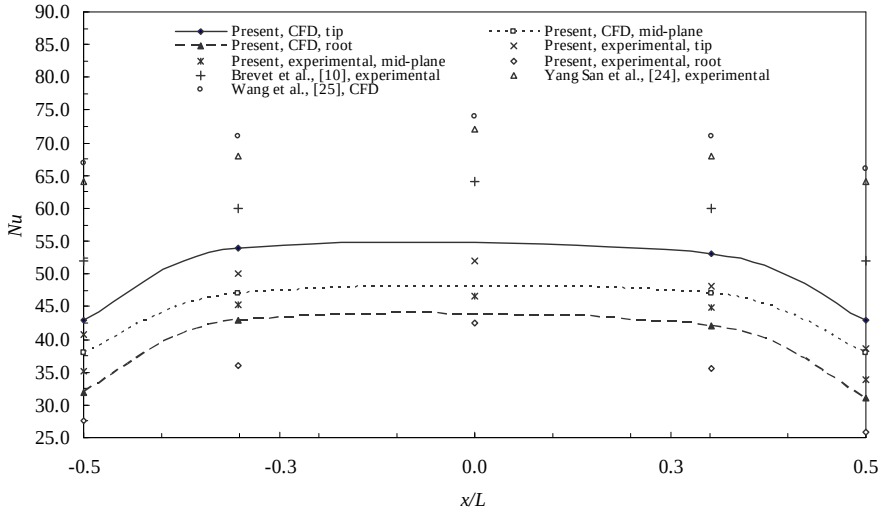

Figure (26), Comparison among present experimental results, CFD ones and previous work of the literature.

خصائص التبريد لسطح مزعنف ومجوف جزئيا نتيجة تعرضه لتدفق نافورة من الهواء

يقدم هذا البحث دراسة عملية وعددية لتحديد خصائص التبريد لسطح مزعنف ومجوف جزئيا نتيجة تعرضه لتدفق نافورة من الهواء. تم إعداد عدد ستة عينات اختبار معملية وقد تم اختيار المصب الحراري لجهاز الحاسوب الشخصي مرجعية لهذه العينات. تم قطع تجاويف مركزية بطرق التشغيل المبرمجة في المصب الحراري على شكل اسطوانة وهرم ناقص ذى زاوية رأس متغيرة. تم أعداد تختة اختبار معملية لاختبار هذه العينات. تم توضيح تأثير كلا من رقم رينولدز وزاوية التصدي والمسافة العمودية بين مخرج النافورة وسطح العينة وشكل التجويف الهندسي على خصائص التبريد. تم توصيف النتائج المعملية في معادلات وضعية لا بعدية. تم محاكاة الدراسة نظريا عن طريق وضع معادلات تفاضلية جزئية ثلاثية البعد وقد تم حل تلك المعادلات عدديا باستخدام CFD FLUENT-6.2-Code وقد تم التأكد من صلاحية النتائج النظرية عن طريق مقارنتها بنظائرها المعملية عند نفس ظروف الاختبارات المعملية. وقد أسفرت هذه الدراسة عن تحسن ملحوظ في خصائص التبريد للمصب الحراري المجوف جزئيا عن نظيره الغير مجوف.